

In vitro Characterization of the Regional Binding Distribution of Amyloid PET Tracer Florbetaben and the Glia Tracers Deprenyl and PK11195 in Autopsy Alzheimer's Brain Tissue

Ruiqing Ni^a, Jennie Rödner^a, Larysa Voytenko^a, Thomas Dyrks^b, Andrea Thiele^b, Amelia Marutle^a and Agneta Nordberg^{a,c,*}

^aDivision of Clinical Geriatrics, Center for Alzheimer Research, Department of Neurobiology, Care Sciences and Society, Karolinska Institutet, Stockholm, Sweden

^bBayer Pharma AG, Berlin, Germany

^cTheme Aging, The Aging Brain Unit, Karolinska University Hospital, Stockholm, Sweden

Accepted 10 February 2021

Pre-press 16 March 2021

Abstract.

Background: Emerging evidence indicates a central role of gliosis in Alzheimer's disease (AD) pathophysiology. However, the regional distribution and interaction of astroglia and microglia in association with amyloid- β ($A\beta$) still remain uncertain.

Objective: Here we studied the pathological profiles in autopsy AD brain by using specific imaging tracers.

Methods: Autopsy brain tissues of AD ($n = 15$, age 70.4 ± 8.5 years) and control cases ($n = 12$, age 76.6 ± 10.9) were examined with homogenate binding assays, autoradiography for $A\beta$ plaques (3H -florbetaben/ 3H -PIB), astroglia (3H -L-deprenyl), and microglia (3H -PK11195/ 3H -FEMPA), as well as immunoassays.

Results: *In vitro* saturation analysis revealed high-affinity binding sites of 3H -florbetaben, 3H -L-deprenyl, and 3H -PK11195/ 3H -FEMPA in the frontal cortex of AD cases. *In vitro* 3H -florbetaben binding increased across cortical and subcortical regions of AD compared to control with the highest binding in the frontal and parietal cortices. The *in vitro* 3H -L-deprenyl binding showed highest binding in the hippocampus (dentate gyrus) followed by cortical and subcortical regions of AD while the GFAP expression was upregulated only in the hippocampus compared to control. The *in vitro* 3H -PK11195 binding was solely increased in the parietal cortex and the hippocampus of AD compared to control. The 3H -florbetaben binding positively correlated with the 3H -L-deprenyl binding in the hippocampus and parietal cortex of AD and controls. Similarly, a positive correlation was observed between 3H -florbetaben binding and GFAP expression in hippocampus of AD and control.

Conclusion: The use of multi-imaging tracers revealed different regional pattern of changes in autopsy AD brain with respect to amyloid plaque pathology versus astroglia and microglia.

Keywords: Alzheimer's disease, amyloid-beta peptides, astrocytes, glial fibrillary acid protein, microglia, monoamine oxidase B, positron emission tomography

*Correspondence to: Professor Agneta Nordberg, MD, PhD, Division of Clinical Geriatrics, Center for Alzheimer Research, Department of Neurobiology, Care Sciences and Society, Karolin-

ska Institutet, Neo, 141 52 Stockholm, Sweden. Tel.: +46 8 524 83532; E-mail: Agneta.K.Nordberg@ki.se.

INTRODUCTION

Alzheimer's disease (AD) involves complex pathophysiology, featured by amyloid- β (A β) deposits, neurofibrillary tangles, gliosis, and neural loss. Emerging evidence implies that A β , astrogliosis, and microgliosis play important roles at early phases of AD [1–5]. However, the regional distribution, consequence of gliosis in relation to A β deposits, whether beneficial or harmful, as well as accurate imaging biomarker for gliosis remains elusive.

Autopsy analysis and *in vivo* positron emission tomography (PET) with A β tracers in AD and nondemented control cases [6] have shown that different brain regions develop A β pathology following the hierarchy of neocortical, limbic, and subcortical areas [7–9]. Higher cortical A β loads (retentions) were observed in patients with AD and mild cognitive impairment (MCI) due to AD compared with control [6, 10] by PET using A β tracers such as ^{11}C -PIB [11], ^{18}F -flutemetamol [12], ^{18}F -florbetapir [13], ^{18}F -florbetaben [14–16], and ^{11}C -AZD2184/ ^{18}F -AZD4694 [17]. Robust correlations between PET and A β pathology at autopsy support the specific detection by A β imaging tracers [18–22]. ^{18}F -florbetaben binding *in vivo* correlated strongly with neuritic plaques detected by Bielschowsky-silver staining and 6E10 immunostaining in AD brain [14], and showed no binding to alpha-synuclein or tau pathologies [23]. The *in vitro* regional distribution of ^3H -florbetaben in autopsy AD brain remains to be characterized.

Accurate detection of neuroinflammation and gliosis *in vivo* has been challenging [4, 24]. One reason is that astrocytes and microglia are highly dynamic and heterogeneous in their subtypes, locations, and activation statuses [25]. ^{11}C -deuterium-L-deprenyl (DED) binds to monoamine oxidase-B (MAO-B) overexpressed in reactive astrocytes and has been evaluated as a biomarker for astrogliosis [26–29]. ^{11}C -DED binding increased in MCI with high ^{11}C -PIB retention compared to AD and control subjects. Longitudinal study in patients with autosomal dominant AD showed that ^{11}C -DED binding elevated

at initial disease stage and declined with increasing ^{11}C -PIB binding during progression, suggesting astrogliosis as an early event [3, 30].

Microglia activation has been assessed by PET using translocator protein (TSPO) tracers [31, 32], such as first-generation ^{11}C -PK11195 [33], second-generation ^{11}C -DAA1106 [34], ^{11}C -PBR28 [35], ^{18}F -FEMPA [36], ^{11}C -GE180 [37], and ^{18}F -DPA-714 [38]. Results from TSPO imaging in MCI and AD have been inconclusive: increase or no change in TSPO retention comparing AD to control group has been reported [33, 39–41]. This could be due to several reasons, including 1) tracer specificity [42]; 2) *TSPO rs6971* genetic polymorphism [25, 43]; 3) heterogeneous and dynamic activation status of microglia [44]; and 4) various cellular expression of TSPO.

To understand the regional distribution of fibrillar A β deposits in relation to astro- and microgliosis, we determined the binding of ^3H -florbetaben/ ^3H -PIB, ^3H -L-deprenyl, and ^3H -PK11195/ ^3H -FEMPA in autopsy brain tissues from AD and control cases by using homogenate binding assays, autoradiography, enzyme-linked immunosorbent assay (ELISA) for astrocyte marker glial fibrillary acidic protein (GFAP). This study demonstrates a clear regional correlation between amyloid plaque deposition and astrogliosis in AD.

MATERIALS AND METHODS

AD and control autopsy brains

Fifteen AD cases (mean age 70.4 ± 8.5 years; mean postmortem delay 5.1 ± 0.9 h), each with a clinical diagnosis confirmed by pathological examination (NINCDS-ADRDA criteria), and twelve control cases (mean age 76.6 ± 10.9 years; mean postmortem delay 7.0 ± 3.8 h) were included in this study (Table 1). Early-onset AD (EOAD) and late-onset AD (LOAD) were classified based on the age of on-set of the clinical symptoms (before or after 65 years of age). Autopsy brain tissues from the frontal,

Table 1
Demographics

Group	No. of brains	Age (y)	Sex (F/M)	Disease duration (y)	PM delay (h)	<i>APOE</i> $\epsilon 4$ (0/1/2)	Braak stage (0–6)
AD	15	70.4 ± 8.5	9/6	6.7 ± 2.7	5.1 ± 0.9	4/5/6	4/5/6
EOAD	8	63.8 ± 5.4	5/3	7.4 ± 2.3	4.8 ± 0.9	3/3/2	4/5/6
LOAD	7	78.0 ± 4.4	4/3	5.7 ± 3.0	5.4 ± 0.9	1/2/4	4/5/6
Control	12	76.6 ± 10.9	6/6		7.0 ± 3.8	12/0/0	1/2

EOAD, early onset Alzheimer's disease; LOAD, late onset Alzheimer's disease; PM, postmortem.

parietal and temporal cortices, hippocampus, caudate nucleus, and cerebellum were obtained from the Netherlands Brain Bank (NBB), Netherlands. The disease relevant cortical and subcortical brain regions, as well as the reference brain region in amyloid PET imaging (cerebellum) were selected. All materials had been collected from donors or from whom a written informed consent for a brain autopsy and the use of the materials and clinical information for research purposes had been obtained by the NBB. Frozen brain tissues from the left hemisphere (all cases) were homogenized in ice-cold 5×0.32 M sucrose containing $10 \mu\text{l/ml}$ protease inhibitor; brain tissues from 4 AD and 4 control cases were cryostat sectioned at $10 \mu\text{m}$ and stored at -80°C . Protein concentration was determined using DC protein assay (Bio-Rad Laboratories AB, Sweden). The apolipoprotein E (*APOE*) genotype was determined using an INNO-LIPA ApoE-kit (Innogenetics, Belgium) with genomic DNA extracted from the thalamic tissue of AD and control cases (QIAamp DNA mini kit, Qiagen, Germany).

The study was conducted according to the principles of the Declaration of Helsinki and subsequent revisions. All experiments on autopsied human brain tissue were carried out in accordance with ethical permission obtained from the regional human ethics committee in Stockholm (permission number 2011/962/31-1), the medical ethics committee of the VU Medical Center for the Netherlands Brain Bank tissue (permission no. 1998-06/5).

Materials

^3H -florbetaben ([N-methyl- ^3H]4-[(E)-2-(4-{2-[2-(2-fluoroethoxy)ethoxy]ethoxy}phenyl) ethenyl]-aniline), specific activity(SA) 63.0 Ci/mmol; ^3H -FEMPA ([N-methyl- ^3H]2-(2-Fluoroethoxy)-5-methoxybenzyl)-N-{2-[(4-methoxyphenyl)oxy]pyridine-3-yl}-acetamide), SA 38.7 Ci/mmol; and unlabeled florbetaben were custom synthesized by Bayer AG, Germany. ^3H -L-deprenyl (N-Methyl- ^3H Hydrochloride), SA 80.0 Ci/mmol, was purchased from American radiolabeled chemicals, USA. ^3H -PK11195 (1-(2-Chlorophenyl)-N-methyl-N-(1-methylpropyl)-3-isoquinolinecarbox-amide), SA 81.7 Ci/mmol, was purchased from Perkin Elmer, USA. ^3H -PIB [N-methyl- ^3H]2-(4'-Methylaminophenyl)-6-hydroxybenzo-thiazole), SA 85.0 Ci/mmol, was custom synthesized by GE Healthcare, UK. Unlabelled L-deprenyl, unlabelled PK11195 and 2-(4'-Methylaminophenyl)benzothiazole (BTA-1), bovine

serum albumin (BSA) were purchased from Sigma-Aldrich, USA.

Characterization of ^3H -florbetaben, ^3H -L-deprenyl, ^3H -FEMPA, and ^3H -PK11195 binding properties in AD and control brains

Saturation binding assays with ^3H -florbetaben (SA 63.0 Ci/mmol) were performed in the frontal cortex homogenates of AD ($n=3$) and control cases ($n=3$) by incubation in 0.1 M PBS + 0.1 % BSA buffer (pH 7.4) containing 0.01–40 nM ^3H -florbetaben for 3 h in tubes at room temperature (RT). Incubations were terminated by filtering samples through Whatman GF/C glass filters pre-soaked with 0.3% polyetylenamine solution. The filters were then washed $3 \times$ ice-cold 0.1 M PBS buffer (pH 7.4), transferred to scintillation vials and the radioactivity counted in a LS-6500 liquid scintillation counter (Beckman Coulter AB, Sweden) [45]. All assays were run in triplicates. The ^3H -florbetaben specific binding was calculated as the difference between total (Non-specific (NSP) binding in the presence of $0.75 \mu\text{M}$ unlabelled florbetaben) and expressed as pmol/g tissue.

Saturation binding assays with ^3H -L-deprenyl (SA 80.0 Ci/mmol) were performed in the frontal cortex homogenate of AD cases ($n=7$) by incubation in ice-cold 0.1 M $\text{Na}^+ \text{-K}^+$ buffer (pH 7.4) containing 0.01–25 nM ^3H -L-deprenyl for 2 h at 37°C (NSP binding in the presence of $1 \mu\text{M}$ unlabelled L-deprenyl). The termination of incubation and counting is the same as aforementioned, except washing $3 \times$ ice-cold 0.1 M $\text{Na}^+ \text{-K}^+$ buffer (pH 7.4). Saturation binding assays with ^3H -PK11195 (SA 81.7 Ci/mmol) and ^3H -FEMPA (SA 38.7 Ci/mmol) were performed in the frontal cortex homogenates of AD cases ($n=6$) by incubation in 0.1 M Tris-HCl buffer (pH 7.4) containing 0.1–30 nM ^3H -FEMPA or 0.5–120 nM ^3H -PK11195 for 2 h at RT (NSP binding in the presence $10 \mu\text{M}$ unlabeled PK11195). The termination of incubation is the same as aforementioned, except washing $3 \times$ ice-cold 0.1 M Tris-HCl buffer (pH 7.4). The specific binding of ^3H -L-deprenyl, ^3H -FEMPA and ^3H -PK11195 were calculated as the difference between total and NSP binding and expressed as pmol/g protein.

Measurements of regional ^3H -florbetaben (5 nM), ^3H -L-deprenyl (6 nM), ^3H -PK11195 (2.5 nM), and ^3H -FEMPA (2.5 nM) binding were performed in the frontal, parietal, temporal cortex, hippocampus, caudate nucleus, and cerebellum of 12 AD and 12 control cases. The incubation time, incubation buffer, and

washing buffers were same as in aforementioned saturation assay respectively. Measurement of ^3H -PIB (1 nM, SA 85.0 Ci/mmol) binding was performed in the frontal and parietal cortex of the same 12 AD and 12 control cases by incubating in 0.1 M PBS + 0.1% BSA buffer (pH 7.4) for 2 h at RT. NSP binding was determined in the presence of 1 μM BTA-1. The termination and counting procedure for ^3H -PIB is the same as that for ^3H -florbetaben assay. The ^3H -PIB specific binding was calculated as the difference between total and NSP binding and expressed as pmol/g tissue.

ELISA measurement of GFAP level

The level of GFAP expression was determined by using ELISA as described previously [46] in the frontal, parietal, temporal cortex, hippocampus, caudate nucleus of 12 AD and 12 control cases. Brain tissue homogenates were sequentially incubated with monoclonal anti-GFAP antibody (Merck KGaA, Germany), alkaline phosphatase-conjugated anti-mouse IgG (Vector, USA), AP and substrate (p-nitro-phenyl-phosphate; Bio-Rad) in a rabbit anti-GFAP antibody pre-coated (Dako, Denmark) microtiter plate. Optical density was assessed in a microtiter plate reader (Tecan, Switzerland) at 405 nm. The level of GFAP was analyzed using Soft Max Pro Plus software (Molecular Devices, USA).

Autoradiography using ^3H -florbetaben, ^3H -L-deprenyl and ^3H -FEMPA in AD brain tissue slices

Adjacent slices (10 μm) from the frontal cortex ($n=4$ each) and hippocampus ($n=3$ each) of AD and control were dried in RT for 20 min and incubated with 2.5 nM ^3H -florbetaben in 0.1 M PBS + 0.5% BSA buffer (pH 7.4) buffer, 10 nM ^3H -L-deprenyl, and 2.5 nM ^3H -FEMPA in 0.1 M Tris-HCl buffer (pH 7.4) for 1 h with NSP binding determined in the presence of unlabeled 0.75 μM florbetaben, 1 μM L-deprenyl, and 10 μM PK11195, respectively. After incubation, the brain slices were washed in corresponding ice-cold buffer 2 \times 5 min and once in ice-cold dd water. The sections were dried in the hood and were exposed to Fuji BAS-TR2040 phosphor imaging plates (Science Imaging Scandinavia AB, Sweden) together with tritium microscale standards (American Radiolabeled Chemicals); 4 days for ^3H -florbetaben, 20 days for ^3H -FEMPA, and 10 days for ^3H -L-deprenyl. The plates were developed with

a Fujifilm BAS-5000 phosphorimager (Fuji, Japan). Binding density was measured using Multigauge software V3.0 (Fuji, Japan).

Statistical analyses

Data was analyzed using GraphPad Prism software 7.0 (GraphPad Software Inc, USA). K_d and B_{max} values from saturation binding curves were determined using a one-site non-linear fitting model. Non-parametric *t*-test (Mann-Whitney) were used for comparisons between AD and control cases. Two-way ANOVA was used to compare early onset AD, late onset AD and control group. Correlation analyses were performed using Pearson's *r* correlation analysis. Significance level was set at * $p < 0.05$, ** $p < 0.01$, *** $p < 0.001$.

RESULTS

Demographic information

Fifteen AD (9 female/6 male) and twelve control cases (6 female/6 male) were included in this study (Table 1). Among the AD cases, 8 were EOAD and the other 7 were LOAD cases. Among the control cases, 2 were younger than 65 years old, and 10 were older than 65 years old. Age and gender did not significantly differ between AD and control groups analyzed by using *Chi*-squared test. *APOE* $\epsilon 4$ genotyping results showed that AD group consisting of seven $\epsilon 4/4$ carriers, five $\epsilon 3/4$ carriers, and four $\epsilon 4$ non-carriers. All control cases are *APOE* $\epsilon 4$ non-carriers.

Binding characterization

Saturation binding studies with ^3H -florbetaben at 0.01–40 nM revealed a high-affinity binding site of $K_d = 11.8 \pm 1.4$ nM in the frontal cortex of AD by non-linear fitting (Table 2). Saturation binding studies with ^3H -L-deprenyl at 0.01–25 nM revealed a high-affinity binding site of $K_d = 10.2 \pm 0.8$ nM in the frontal cortex of AD cases ($n=7$) (Table 2). The non-specific binding was approx. 5% for ^3H -L-deprenyl. Saturation binding studies with ^3H -PK11195 at 0.5–40 nM and ^3H -FEMPA at 0.1–30 nM revealed similar high-affinity binding site of 1.8 ± 0.6 nM and 3.3 ± 0.1 nM respectively in the frontal cortex of AD cases ($n=6$) by non-linear fitting (Table 2, Supplementary Figure 1). The non-specific binding was less than 10% for both ^3H -PK11195 and ^3H -FEMPA.

Different regional ^3H -florbetaben, ^3H -L-deprenyl, ^3H -PK11195, and GFAP distribution in AD and control brain

^3H -florbetaben (5 nM) showed significant increases in the frontal cortex ($p < 0.001$), followed by the parietal cortex ($p < 0.001$), temporal cortex ($p < 0.001$), caudate nucleus ($p < 0.001$), and hippocampus ($p = 0.0387$) of AD ($n = 12$) compared to control ($n = 12$) (Fig. 1a). ^3H -L-deprenyl (6 nM) showed significant increases in the hippocampus ($p = 0.0002$)

Table 2
Binding properties for ^3H -florbetaben, ^3H -L-deprenyl, ^3H -FEMPA, and ^3H -PK11195 in the frontal cortex of AD cases

Tracer	K_d (nM)	B_{max} (pmol/g tissue or protein)
^3H -florbetaben ($n = 3$)	11.8 ± 1.4	2146 ± 964
^3H -L-deprenyl ($n = 7$)	10.2 ± 0.8	322 ± 47
^3H -FEMPA ($n = 6$)	3.3 ± 0.1	251 ± 147
^3H -PK11195 ($n = 6$)	1.8 ± 0.6	355 ± 139

K_d , dissociation constant; B_{max} , maximum number of binding sites. Results are expressed as mean \pm standard deviation.

followed by the temporal cortex ($p = 0.0014$), the frontal and parietal cortex ($p = 0.0284$, $p = 0.0121$), and caudate nucleus ($p = 0.0374$) of AD ($n = 11-12$) compared to control cases ($n = 12$) (Fig. 1b). 2.5 nM ^3H -PK11195 showed significant increases in the parietal cortex ($p = 0.0332$) and hippocampus ($p = 0.0317$) of AD ($n = 12$) compared with control ($n = 12$) (Fig. 1c). In comparison, another TSPO tracer ^3H -FEMPA (2.5 nM) did not show difference in any brain regions between AD and control (Supplementary Figure 1). The levels of GFAP expression were determined by ELISA in five brain regions of the same AD ($n = 12$) and control ($n = 12$) cases included in binding assays. The levels of GFAP expression significantly increased in the hippocampus ($p = 0.0280$) of AD compared to control (Fig. 1d), and not in the other regions.

The difference between EOAD, LOAD, and control group was analyzed using two-way ANOVA comparison (Table 3). High ^3H -florbetaben binding was observed in all three cortical regions in EOAD and LOAD compared to control. The ^3H -L-deprenyl

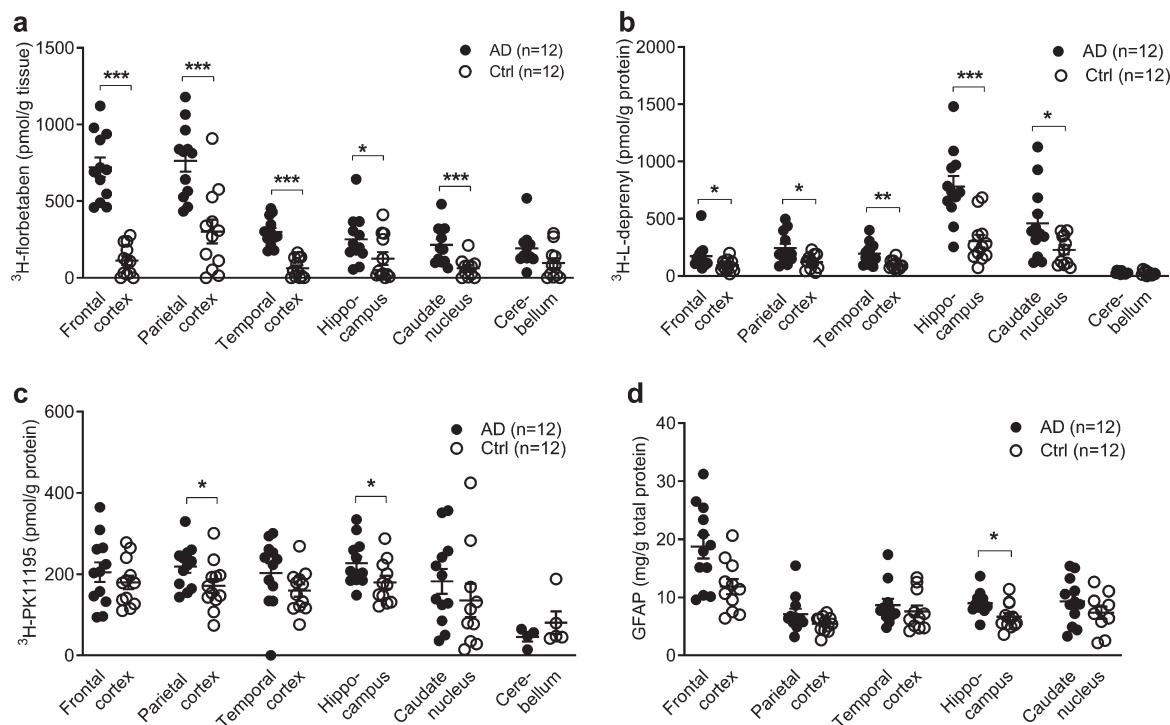


Fig. 1. Regional ^3H -florbetaben, ^3H -L-deprenyl, ^3H -PK11195 binding and level of GFAP expression in AD and control brain. a) ^3H -florbetaben (5 nM) binding in the brain homogenate from AD and control cases. b) ^3H -L-deprenyl (6 nM) binding in brain tissue homogenates from AD and control cases. c) ^3H -PK11195 (2.5 nM) binding in brain tissue homogenates from AD and control cases. d) Level of GFAP expression in the same AD and control cases; Significant differences between AD and control groups are indicated by * $p < 0.05$, ** $p < 0.01$ and *** $p < 0.001$.

Table 3
Comparison of ^3H -florbetaben, ^3H -L-deprenyl, ^3H -FEMPA, and ^3H -PK11195 binding between EOAD, LOAD and control

Tracer	Region	Group			p		
		EOAD ($n=7$)	LOAD ($n=5$)	Ctrl ($n=12$)	EOAD versus Ctrl	LOAD versus Ctrl	EOAD versus LOAD
^3H -L-deprenyl	PC	187 \pm 66	322 \pm 175	138 \pm 55	ns	0.0183	ns
	HIP	662 \pm 214	946 \pm 387	301 \pm 191	<0.0001	<0.0001	0.0004
	CN	546 \pm 381	342 \pm 153	245 \pm 125	<0.0001	ns	0.0168
^3H -florbetaben	FC	737 \pm 210	698 \pm 256	113 \pm 100	<0.0001	<0.0001	Ns
	PC	804 \pm 200	705 \pm 302	302 \pm 269	<0.0001	<0.0001	Ns
	TC	315 \pm 95	277 \pm 97	64 \pm 64	0.0001	0.0047	Ns
	HIP	274 \pm 171	210 \pm 118	125 \pm 145	0.0366	ns	Ns

CN, caudate nucleus; Ctrl, control; EOAD, early onset Alzheimer's disease; HIP, hippocampus; LOAD, late onset Alzheimer's disease; ns, not significant; PC, parietal cortex; TC, temporal cortex. Values represent Mean \pm standard deviation.

binding was higher in the hippocampus while lower in the caudate nucleus of LOAD compared to EOAD. No difference was observed in the regional ^3H -florbetaben, or ^3H -PK11195 binding between EOAD and LOAD group.

Autoradiography showed high ^3H -florbetaben in the cortex, and ^3H -L-deprenyl signal in the dentate gyrus

Autoradiography using ^3H -florbetaben (2.5 nM) showed increased signal in the grey matter in the frontal cortex slices from AD compared to control cases ($p < 0.05$) (Fig. 2a, d). To further analyze the sub-regional distribution of ^3H -L-deprenyl binding, autoradiography using ^3H -L-deprenyl (10 nM) was performed in the frontal cortex and hippocampus slices from three AD and three control cases (Fig. 2b, c). ^3H -L-deprenyl binding was higher in the dentate gyrus of AD compared to control cases ($p = 0.0306$, Fig. 2e). A laminar pattern of ^3H -L-deprenyl binding was observed in the frontal cortex (Fig. 2b) which was not observed for ^3H -florbetaben (Fig. 2a).

Correlation analysis

To investigate the relation between the levels of different readouts in AD and control, Pearson's r correlation analysis was performed. The ^3H -florbetaben binding positively correlated with ^3H -L-deprenyl binding in the hippocampus, parietal and temporal cortex of AD and control cases (Fig. 3a-c). No significant correlation was observed between ^3H -florbetaben and ^3H -PK1195 binding in the hippocampus (data not shown). ^3H -PIB (1 nM) binding measured in the frontal cortex and parietal cortex showed significant increases in AD ($n=12$) compared to control cases ($n=12$, $p < 0.001$); and

correlating with ^3H -florbetaben binding respectively (Supplementary Figure 2a, b).

We analyzed the correlation between different readouts across the whole brain. Correlations were observed between ^3H -PK11195 and ^3H -L-deprenyl binding ($p = 0.042$, $r = 0.5934$) in the six brain regions (frontal, parietal, temporal cortex, hippocampus, caudate nucleus and cerebellum) as well as between ^3H -PK11195 and ^3H -florbetaben binding in AD and control groups across five brain regions (frontal, parietal, temporal cortex, hippocampus, and caudate nucleus) (Fig. 4a, b).

DISCUSSION

Cellular events such as abnormal A β and tau accumulation, dystrophic neurites, reactive astrocytes, and microglia contribute to the pathogenesis of AD. Different pathological subtypes of AD, with/without abnormal A β accumulation have been documented [2, 47, 48]. Regional characterization of different molecular pathology profiles in autopsy AD brain thus provides insights into the disease mechanism [49] as well as validation for imaging biomarkers [19, 50]. Here we demonstrated distinct region-specific distributions of A β deposits (^3H -florbetaben), astrogliosis (^3H -L-deprenyl, GFAP) and activated microglia (^3H -PK11195) in AD brain.

We showed that regional ^3H -florbetaben binding corresponded to the known high cortical and low hippocampal A β deposits pattern in AD brain. Good *in vivo* ^{18}F -florbetaben PET-A β histopathology correspondence, specific detection of cerebral A β deposits in AD [14, 51–53] has been reported from recent phase III studies. Our results of strong correlation of ^3H -florbetaben and ^3H -PIB binding is in line with reported comparable binding properties of the tracers [54, 55], and *in vivo* ^{11}C -PIB

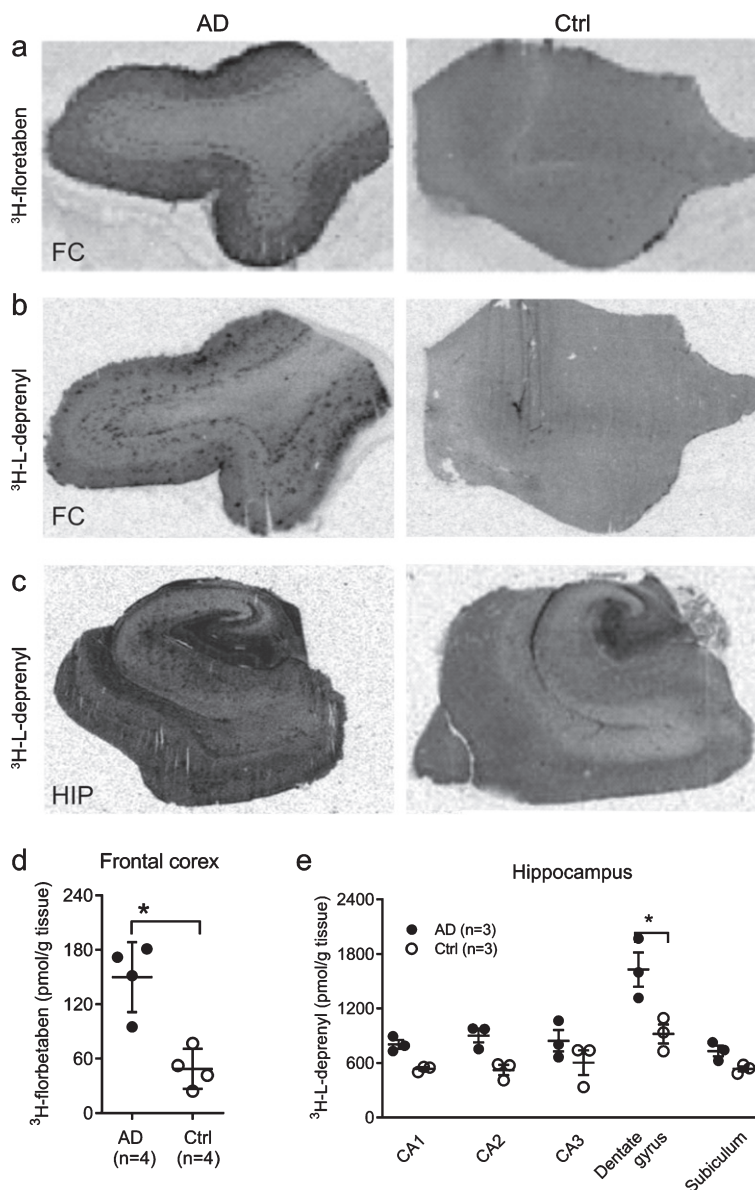


Fig. 2. Autoradiography using ^3H -florbetaben and ^3H -L-deprenyl in AD and control brain. Autoradiography and quantification in AD ($n = 3$) and control cases ($n = 3$), using (a, d) ^3H -florbetaben (5 nM) in the frontal cortex slices; (b-c, e) using ^3H -L-deprenyl (10 nM) in the frontal cortex and the hippocampus slices; Significant differences between AD and control groups are indicated by $*p < 0.05$.

and ^{18}F -florbetaben PET head-to-head comparison results [56, 57]. The low hippocampal ^3H -florbetaben binding in this study has been observed by *in vivo* PET using ^{18}F -florbetaben [14] and ^{11}C -PIB [58]. The amyloid tracer binding might differ from the pathological observations on the autopsy brain tissues that A β deposits accumulate in hippocampus at early phase II Thal stage [9]. One possible explanation is that the hippocampal A β deposits consist of more diffuse and oligomeric A β with lower amount

of β -sheet structures. Thus the β -sheet binding amyloid PET tracers show mainly low-affinity binding site as compared to the major high-affinity binding sites in the cortical AD brain tissues [9, 54].

Astrocytes play an important role in the brain physiology, as well as in learning and memory formation [59]. Reactive astrogliosis are dynamic and heterogeneous in their location, subtypes, hypertrophy/proliferation, and upregulation of different markers such as GFAP, vimentin, nestin, MAO-B,

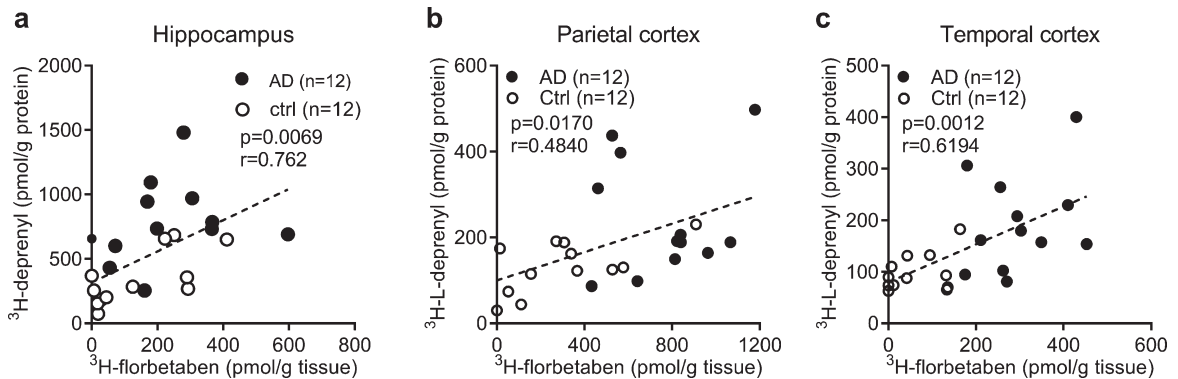


Fig. 3. Correlation between regional ^3H -florbetaben, ^3H -L-deprenyl binding and level of GFAP expression in AD and control brain. a-c) Correlation between ^3H -L-deprenyl (6 nM) and ^3H -florbetaben (5 nM) binding in the hippocampus, parietal and temporal cortex of AD and control cases.

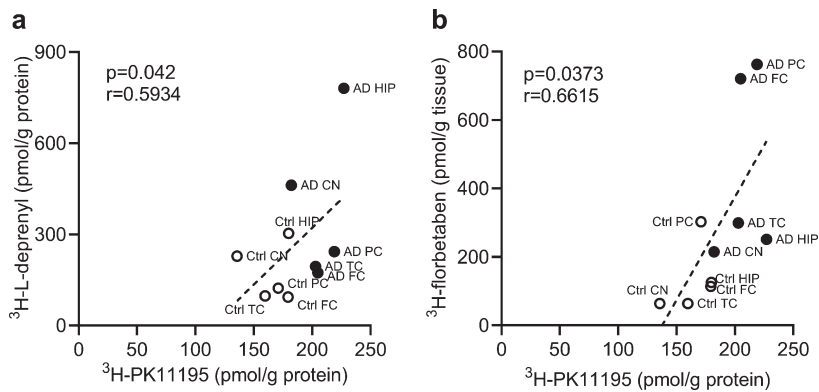


Fig. 4. Correlation between regional ^3H -PK11195, ^3H -florbetaben, and ^3H -L-deprenyl binding in AD and control brain. a) Correlation between ^3H -PK11195 (2.5 nM) and ^3H -L-deprenyl (6 nM) binding across the six brain regions: frontal cortex (FC), parietal cortex (PC), temporal cortex (TC), hippocampus (HC), caudate Nucleus (CN), and cerebellum (CN). b) Correlation between ^3H -PK11195 (2.5 nM) and ^3H -florbetaben (5 nM) binding across the five brain regions: FC, PC, TC, HC, and CN.

and gamma-amino butyric acid [60, 61]. Reactive astrocytes have been shown play an important role early in the development of AD [62, 63]. Elevated ^3H -L-deprenyl (MAO-B) measures of astrogliosis was observed in the hippocampus especially in the dentate gyrus, followed by the cortical regions of AD, consistent with autopsy [50, 64, 65] and *in vivo* ^{11}C -DED PET evidence [3]. The similar regional distribution pattern for amyloid plaques (^3H -florbetaben) and astrogliosis (^3H -L-deprenyl) may suggest a close relationship in AD pathology. However, a regional difference was observed with high astrogliosis measured in the hippocampus (dentate gyrus), a region with low amyloid plaque load. ^3H -L-deprenyl showed a laminar binding pattern in the frontal cortex of AD which was absent for the amyloid plaque tracer ^3H -florbetaben binding. This observation is consistent with earlier studies using

^3H -L-deprenyl/ ^3H -PIB [50] in the autopsy AD brain: ^3H -L-deprenyl binding distributes in all layer in hippocampus and superficial layer in frontal cortex of AD brain, while ^3H -PIB binding spreads in the all layers in the frontal cortex.

Regional GFAP expression seems to differ from ^3H -L-deprenyl binding in AD brains. In comparison to ^3H -L-deprenyl binding, the GFAP expression is most elevated in the frontal cortex of AD and a positive correlation with ^3H -L-deprenyl was only observed in the hippocampus. Different distribution patterns of GFAP and ^3H -L-deprenyl were also observed in brain of Tg2576 mouse model of AD [66]. These two methods might detect different status/types of astrogliosis, as 1) GFAP is expressed non-uniformly on subtypes of astrocytes [67]; 2) change in glia phenotype profiles but not number of GFAP + astrocytes in AD brain; 3) MAO-B expressed

in astrocytes as well as in dopaminergic neurons mainly in subcortical regions.

We found similar high affinities of ^3H -PK11195 and ^3H -FEMPA in the cortex of AD, in line with reported high-affinity binding sites of ^3H -PK11195 [43] and ^{18}F -FEMPA [36]. The presence of subjects with mixed binding sites of ^3H -FEMPA may lead to the observed larger variation in binding distribution compared to ^3H -PK11195. ^3H -PK11195 shows highest binding in the temporal cortex and hippocampus that is markedly affected by tau aggregates as shown by histopathology [68] and in PET investigations [69, 70]. ^{11}C -PK11195 is the first PET tracer for TSPO imaging. Despite its limitations including a short half-life, relatively low brain uptake, suboptimal metabolic profile, high non-specific binding, ^{11}C -PK11195 is still currently the most used TSPO tracer in AD research. The level of ^{11}C -PK11195 and amyloid load measured by ^{11}C -PIB in AD patients were positively correlated within the frontal, parietal and temporal cortices [71, 72]. Recent study using autopsy brain tissues suggest an overlap in the levels of TSPO protein and mRNA between AD and healthy-control, and a limited influence by *TSPO rs6971* polymorphism [43]. Novel TSPO tracers with improved binding specificity, SNR and higher brain uptake was pursued, such as ^{18}F -GE-180 [73], ^{11}C -PBR28 [74], ^{11}C -DAA1106 [34], ^{11}C -vinpocetine [75], ^{18}F -DPA-714 [76], ^{18}F -FEPPA [77], and ^{11}C -AC5216 [78]. In addition, new tracers for imaging neuroinflammation beyond TSPO are under development for microgliosis [79, 80] and astrogliosis [4] (including novel MAO-B tracer [81]). Elucidating the cellular origin of the radiotracer binding such as TSPO binding [82] and whether they are selective for pro-inflammatory astrocytes and microglia will be critical [83].

We observe a similar higher regional ^3H -florbetaben binding in EOAD and LOAD cases, compared to control cases. This is in line with previous observation by *in vivo* ^{11}C -PIB imaging in EOAD and LOAD patients showing comparable amyloid load [84]. Interestingly the ^3H -L-deprenyl binding was higher in the hippocampus of LOAD compared to EOAD, and lower in the caudate nucleus of LOAD compared to EOAD. For cerebral glucose metabolism (^{18}F -FDG PET), a more pronounced hypometabolism has been reported in EOAD compared to LOAD [84]. Similarly, a higher *in vivo* binding of tau PET tracers as well as *in vitro* tau tracer binding have been observed in EOAD compared to LOAD patients [85]. Both FDG and tau tracer

binding could be explained by a more pronounced AD pathology in EOAD compared to LOAD. It can be speculated that the finding in this study of higher astrogliosis (higher ^3H -L-deprenyl binding) in the hippocampus of LOAD compared to EOAD might be due to more hippocampus sparing cases [86] in the EOAD group which might explain the lower astrogliosis in EOAD compared to LOAD. An increased ^{11}C -DED binding has also been demonstrated in brain by PET in aging [87].

Positive correlations between ^3H -florbetaben-GFAP and ^3H -florbetaben- ^3H -L-deprenyl were observed in the hippocampus, parietal cortex, and temporal cortex in the current study. This corresponds to the reported ^3H -PIB-GFAP correlation in sporadic AD autopsy brain [19]. However, negative $\text{A}\beta_{40}$ -GFAP correlation in both sporadic and familial AD have also been reported [49]. In addition, ^3H -PK11195 binding positively correlates with ^3H -florbetaben in five brain regions and ^3H -L-deprenyl binding in all six brain regions. This corresponds to the reported positive ^{11}C -PIB- ^{11}C -PK11195 correlation in AD cases [88]. The regional link between ^3H -florbetaben- ^3H -L-deprenyl appears stronger than ^3H -florbetaben- ^3H -PK11195 (Fig. 3). Reactive astrocytes and activated microglia were observed in the vicinity of $\text{A}\beta$ plaques in the AD frontal cortex [89]. Microglial innate immune responses are highly versatile in AD, producing an array of proinflammatory cytokines and mediators in response to $\text{A}\beta$. These proinflammatory changes activates astrocytes, which in turn secretes cytokines such as interleukin-1 and TNF-alpha. Thus, a vicious neuroinflammatory cycle occurs that initiates and propels disease forward to widespread circuits that undergo dysfunction at a later stage.

Regions within the default-mode network (DMN) are highly overlapping with the spatial distribution of both $\text{A}\beta$ and tau pathologies detected by using PET [90–94]. The degree of alterations to DMN connectivity has also been found relating to disease progression [92]. The spread of amyloid pathology from the medial temporal lobe has been found associated with glucose metabolism measured by ^{18}F -FDG PET [95, 96].

This study presents the binding properties of different PET tracers for detecting different AD pathologies. We have to conclude that investigations in autopsy AD brain tissues represent the status at final stage of AD. This is in contrast to *in vivo* PET and MRI studies [3, 4], where the regional rate of deposit of different pathological markers including amyloid

plaque load, tau, astrogliosis, and microglia activation, and neurodegeneration in form of hypoglycose metabolism and structural changes (atrophy) can be measured during the time course of the disease from preclinical stages, defined also by the ATN criteria [10]. In addition, there is a rapid development in the field of imaging biomarkers in AD for amyloid-beta, tauopathy [97, 98], neuroinflammation as well as synaptic density measurement [99]. Magnetic resonance imaging diffusion basis spectrum imaging has been used to detect indicators of neuroinflammation in AD, provide further insight into white matter microstructural integrity [100, 101].

There are several limitations of the study. Firstly, additional *TSPO* gene *rs6971* polymorphism data could be useful for categorizing ^3H -FEMPA high/mixed/low-affinity binders. Secondly, with regards to astrocyte and microglia subtypes [82], immunohistochemical staining with multiple antibodies such as glutamate synthases for astrocyte and MHC-II for microglia, as well as morphology study for resting versus activating subtypes. Thirdly, difference between the binding properties measured in autoradiography and homogenate assays remains unclear. One explanation is that *TSPO* and *MAO-B*, which both locates in the mitochondria, exposes to tracers at different degrees depending on the method adopted [65]. Parallel regional characterization with tau tracers and additional tracers for neuroinflammation will provide with a more comprehensive picture of the pathology in AD brain [69, 70, 102]. Fourthly, regional binding studies with tau PET tracers would have most probably provided valuable data especially regarding binding properties in AD hippocampus and temporal cortices. Unfortunately, we did not have access to any ^3H -labelled tau tracer when the studies were performed.

CONCLUSIONS

Our results showed a different regional profile of $\text{A}\beta$ plaque deposits versus astrogliosis and microgliosis; and supported the specific measurement by ^3H -florbetaben, ^3H -L-deprenyl, GFAP expression, and ^3H -PK11195 binding in AD and control brains. A clear relationship was observed between $\text{A}\beta$ plaque deposition and astrogliosis in AD hippocampus which was not observed for microgliosis. Developing of more specific tracers for disease-relevant gliosis will improve the development of new PET tracers for studies of neuroglia in AD and thereby provide a

further understanding of early disease mechanisms important early detection and diagnosis and new treatment targets in AD.

ACKNOWLEDGMENTS

This work was financially supported by a research agreement between Karolinska Institutet and Bayer AG, Pharmaceuticals, Berlin, Germany, the Swedish Foundation for Strategic Research (RB13-0192), the Swedish Research Council (project 05817, 2017-0295, 2017-06086), the Stockholm County Council-Karolinska Institutet regional agreement on medical training and clinical research (ALF grant), the Swedish Brain Foundation, the Alzheimer Foundation in Sweden, and Center for Innovative Medicine, Karolinska Institutet (CIMED).

Authors' disclosures available online (<https://www.j-alz.com/manuscript-disclosures/20-1344r2>).

SUPPLEMENTARY MATERIAL

The supplementary material is available in the electronic version of this article: <https://dx.doi.org/10.3233/JAD-201344>.

REFERENCES

- [1] Heneka MT, Carson MJ, El Khoury J, Landreth GE, Brosseron F, Feinstein DL, Jacobs AH, Wyss-Coray T, Vitorica J, Ransohoff RM, Herrup K, Frautschy SA, Finsen B, Brown GC, Verkhratsky A, Yamanaka K, Koistinaho J, Latz E, Halle A, Petzold GC, Town T, Morgan D, Shinohara ML, Perry VH, Holmes C, Bazan NG, Brooks DJ, Hunot S, Joseph B, Deigendesch N, Garaschuk O, Boddeke E, Dinarello CA, Breitner JC, Cole GM, Golenbock DT, Kummer MP (2015) Neuroinflammation in Alzheimer's disease. *Lancet Neurol* **14**, 388-405.
- [2] Serrano-Pozo A, Betensky RA, Frosch MP, Hyman BT (2016) Plaque-associated local toxicity increases over the clinical course of Alzheimer disease. *Am J Pathol* **186**, 375-384.
- [3] Rodríguez-Vieitez E, Saint-Aubert L, Carter SF, Almkvist O, Farid K, Scholl M, Chiotis K, Thordardottir S, Graff C, Wall A, Langstrom B, Nordberg A (2016) Diverging longitudinal changes in astrocytosis and amyloid PET in autosomal dominant Alzheimer's disease. *Brain* **139**, 922-936.
- [4] Carter SF, Herholz K, Rosa-Neto P, Pellerin L, Nordberg A, Zimmer ER (2019) Astrocyte biomarkers in Alzheimer's disease. *Trends Mol Med* **25**, 77-95.
- [5] Arranz AM, De Strooper B (2019) The role of astroglia in Alzheimer's disease: Pathophysiology and clinical implications. *Lancet Neurol* **18**, 406-414.
- [6] Villemagne VL, Burnham S, Bourgeat P, Brown B, Ellis KA, Salvado O, Szoek C, Macaulay SL, Martins R, Maruff P, Ames D, Rowe CC, Masters CL (2013) Amyloid beta deposition, neurodegeneration, and cognitive decline

- in sporadic Alzheimer's disease: A prospective cohort study. *Lancet Neurol* **12**, 357-367.
- [7] Thal DR, Rub U, Orantes M, Braak H (2002) Phases of A beta-deposition in the human brain and its relevance for the development of AD. *Neurology* **58**, 1791-1800.
- [8] Murray ME, Lowe VJ, Graff-Radford NR, Liesinger AM, Cannon A, Przybelski SA, Rawal B, Parisi JE, Petersen RC, Kantarci K, Ross OA, Duara R, Knopman DS, Jack CR, Jr., Dickson DW (2015) Clinicopathologic and 11C-Pittsburgh compound B implications of Thal amyloid phase across the Alzheimer's disease spectrum. *Brain* **138**, 1370-1381.
- [9] Thal DR, Rüb U, Schultz C, Sassin I, Ghebremedhin E, Del Tredici K, Braak E, Braak H (2000) Sequence of A β -protein deposition in the human medial temporal lobe. *J Neuropathol Exp Neurol* **59**, 733-748.
- [10] Jack CR, Jr., Bennett DA, Blennow K, Carrillo MC, Dunn B, Haeberlein SB, Holtzman DM, Jagust W, Jessen F, Karlawish J, Liu E, Molinuevo JL, Montine T, Phelps C, Rankin KP, Rowe CC, Scheltens P, Siemers E, Snyder HM, Sperling R (2018) NIA-AA Research Framework: Toward a biological definition of Alzheimer's disease. *Alzheimers Dement* **14**, 535-562.
- [11] Klunk WE, Engler H, Nordberg A, Wang Y, Blomqvist G, Holt DP, Bergstrom M, Savitcheva I, Huang GF, Estrada S, Ausen B, Debnath ML, Barletta J, Price JC, Sandell J, Lopresti BJ, Wall A, Koivisto P, Antoni G, Mathis CA, Langstrom B (2004) Imaging brain amyloid in Alzheimer's disease with Pittsburgh Compound-B. *Ann Neurol* **55**, 306-319.
- [12] Curtis C, Gamez JE, Singh U, Sadowsky CH, Villena T, Sabbagh MN, Beach TG, Duara R, Fleisher AS, Frey KA, Walker Z, Hunjan A, Holmes C, Escovar YM, Vera CX, Agronin ME, Ross J, Bozoki A, Akinola M, Shi J, Vandenberghe R, Ikonovic MD, Sherwin PF, Grachev ID, Farrar G, Smith AP, Buckley CJ, McLain R, Salloway S (2015) Phase 3 trial of flutemetamol labeled with radioactive fluorine 18 imaging and neuritic plaque density. *JAMA Neurol* **72**, 287-294.
- [13] Johnson KA, Sperling RA, Gidicsin CM, Carmasin JS, Maye JE, Coleman RE, Reiman EM, Sabbagh MN, Sadowsky CH, Fleisher AS, Murali Doraiswamy P, Carpenter AP, Clark CM, Joshi AD, Lu M, Grundman M, Mintun MA, Pontecorvo MJ, Skovronsky DM, AV45-A11 study group (2013) Florbetapir (F18-AV-45) PET to assess amyloid burden in Alzheimer's disease dementia, mild cognitive impairment, and normal aging. *Alzheimers Dement* **9**(5 Suppl), S72-83.
- [14] Sabri O, Sabbagh MN, Seibyl J, Barthel H, Akatsu H, Ouchi Y, Senda K, Murayama S, Ishii K, Takao M, Beach TG, Rowe CC, Leverenz JB, Ghetti B, Ironside JW, Catafau AM, Stephens AW, Mueller A, Koglin N, Hoffmann A, Roth K, Reiningger C, Schulz-Schaeffer WJ, Florbetaben Phase 3 Study Group (2015) Florbetaben PET imaging to detect amyloid beta plaques in Alzheimer's disease: Phase 3 study. *Alzheimers Dement* **11**, 964-974.
- [15] Ceccaldi M, Jonveaux T, Verger A, Krolak-Salmon P, Houzard C, Godefroy O, Shields T, Perrotin A, Gismondi R, Bullich S, Jovalekic A, Raffa N, Pasquier F, Semah F, Dubois B, Habert M-O, Wallon D, Chastan M, Payoux P, Ceccaldi M, Guedj E, Ceccaldi M, Felician O, Didic M, Gueriot C, Koric L, Kletchkova-Gantchev R, Guedj E, Godefroy O, Andriuta D, Devendeville A, Dupuis D, Binot I, Barbay M, Meyer M-E, Moullard V, Magnin E, Chamard L, Haffen S, Morel O, Drouet C, Boulahdour H, Goas P, Querellou-Lefranc S, de la Sayette V, Cogez J, Branger P, Agostini D, Manrique A, Rouaud O, Bejot Y, Jacquin-Piques A, Dygai-Cochet I, Berriolo-Riedinger A, Moreaud O, Sauvee M, Crépin CG, Pasquier F, Bombois S, Lebouvier T, Mackowiak-Cordoliani M-A, Deramecourt V, Rollin-Sillaire A, Cassagnaud-Thuillet P, Chen Y, Semah F, Petyt G, Krolak-Salmon P, Federico D, Danaila KL, Guilhermet Y, Magnier C, Makaroff Z, Rouch I, Xie J, Roubaud C, Coste M-H, David K, Sarciron A, Waissi AS, Scheiber C, Houzard C, Gabelle-Deloustal A, Bennys K, Marelli C, Touati L, Mariano-Goulart D, de Verbizier-Lonjon D, Jonveaux T, Benetos A, Kearney-Schwartz A, Perret-Guillaume C, Verger A, Vercelletto M, Boutoleau-Bretonniere C, Pouclet-Courtemanche H, Wagemann N, Pallardy A, Hugon J, Paquet C, Dumurgier J, Millet P, Queneau M, Dubois B, Epelbaum S, Levy M, Habert M-O, Novella J-L, Jaidi Y, Papathanassiou D, Morland D, Belliard S, Salmon A, Lejeune F, Hannequin D, Wallon D, Martinaud O, Zarea A, Chastan M, Pariente J, Thalamas C, Galitzky-Gerber M, Tricoire Ricard A-M, Calvas F, Rigal E, Payoux P, Hitzel A, Delrieu J, Ousset P-J, Lala F, Sastre-Hengan N, Stephens A, Guedj E (2018) Added value of 18F-florbetaben amyloid PET in the diagnostic workup of most complex patients with dementia in France: A naturalistic study. *Alzheimers Dement* **14**, 293-305.
- [16] Rowe CC, Ackerman U, Browne W, Mulligan R, Pike KL, O'Keefe G, Tochon-Danguy H, Chan G, Berlangieri SU, Jones G, Dickinson-Rowe KL, Kung HP, Zhang W, Kung MP, Skovronsky D, Dyrks T, Holl G, Krause S, Friebe M, Lehman L, Lindemann S, Dinkelborg LM, Masters CL, Villemagne VL (2008) Imaging of amyloid beta in Alzheimer's disease with 18F-BAY94-9172, a novel PET tracer: Proof of mechanism. *Lancet Neurol* **7**, 129-135.
- [17] Cselenyi Z, Jonhagen ME, Forsberg A, Halldin C, Julin P, Schou M, Johnstrom P, Varnas K, Svensson S, Farde L (2012) Clinical validation of 18F-AZD4694, an amyloid-beta-specific PET radioligand. *J Nucl Med* **53**, 415-424.
- [18] Ikonovic MD, Klunk WE, Abrahamson EE, Mathis CA, Price JC, Tsopelas ND, Lopresti BJ, Ziolkowski S, Bi W, Paljug WR, Debnath ML, Hope CE, Isanski BA, Hamilton RL, DeKosky ST (2008) Post-mortem correlates of *in vivo* PiB-PET amyloid imaging in a typical case of Alzheimer's disease. *Brain* **131**, 1630-1645.
- [19] Kadir A, Marutle A, Gonzalez D, Scholl M, Almkvist O, Mousavi M, Mustafiz T, Darreh-Shori T, Nennesmo I, Nordberg A (2010) Positron emission tomography imaging and clinical progression in relation to molecular pathology in the first Pittsburgh Compound B positron emission tomography patient with Alzheimer's disease. *Brain* **134**, 301-317.
- [20] Clark CM, Pontecorvo MJ, Beach TG, Bedell BJ, Coleman RE, Doraiswamy PM, Fleisher AS, Reiman EM, Sabbagh MN, Sadowsky CH, Schneider JA, Arora A, Carpenter AP, Flitter ML, Joshi AD, Krautkramer MJ, Lu M, Mintun MA, Skovronsky DM, Group A-AS (2012) Cerebral PET with florbetapir compared with neuropathology at autopsy for detection of neuritic amyloid-beta plaques: A prospective cohort study. *Lancet Neurol* **11**, 669-678.
- [21] Thal DR, Beach TG, Zanette M, Heurling K, Chakraborty A, Ismail A, Smith AP, Buckley C (2015) [(18)F]flutemetamol amyloid positron emission tomography in preclinical and symptomatic Alzheimer's disease: Specific detection of advanced phases of amyloid-beta pathology. *Alzheimers Dement* **11**, 975-985.

- [22] La Joie R, Ayakta N, Seeley WW, Borys E, Boxer AL, DeCarli C, Doré V, Grinberg LT, Huang E, Hwang J-H, Ikonomic MD, Jack C, Jagust WJ, Jin L-W, Klunk WE, Kofler J, Lesman-Segev OH, Lockhart SN, Lowe VJ, Masters CL, Mathis CA, McLean CL, Miller BL, Mungas D, O'Neil JP, Olichney JM, Parisi JE, Petersen RC, Rosen HJ, Rowe CC, Spina S, Vemuri P, Villemagne VL, Murray ME, Rabinovici GD (2019) Multisite study of the relationships between antemortem [^{11}C]PIB-PET Centiloid values and postmortem measures of Alzheimer's disease neuropathology. *Alzheimers Dement* **15**, 205-216.
- [23] Fodero-Tavoletti MT, Brockschneider D, Villemagne VL, Martin L, Connor AR, Thiele A, Berndt M, McLean CA, Krause S, Rowe CC, Masters CL, Dinkelborg L, Dyrks T, Cappai R (2012) *In vitro* characterization of [^{18}F]florbetaben, an Abeta imaging radiotracer. *Nucl Med Biol* **39**, 1042-1048.
- [24] Calsolaro V, Edison P (2016) Neuroinflammation in Alzheimer's disease: Current evidence and future directions. *Alzheimers Dement* **12**, 719-732.
- [25] Jacobs AH, Tavittian B (2012) Noninvasive molecular imaging of neuroinflammation. *J Cereb Blood Flow Metab* **32**, 1393-1415.
- [26] Ekblom J, Jossan SS, Bergstrom M, Orelund L, Walum E, Aquilonius SM (1993) Monoamine oxidase-B in astrocytes. *Glia* **8**, 122-132.
- [27] Saura J, Luque JM, Cesura AM, Da Prada M, Chan-Palay V, Huber G, Löffler J, Richards JG (1994) Increased monoamine oxidase B activity in plaque-associated astrocytes of Alzheimer brains revealed by quantitative enzyme radioautography. *Neuroscience* **62**, 15-30.
- [28] Fowler JS, Logan J, Shumay E, Alia-Klein N, Wang G-J, Volkow ND (2015) Monoamine oxidase: Radiotracer chemistry and human studies. *J Labelled Compd Rad* **58**, 51-64.
- [29] Gulyás B, Pavlova E, Kása P, Gulya K, Bakota L, Várszegi S, Keller É, Horváth MC, Nag S, Hermeicz I, Magyar K, Halldin C (2011) Activated MAO-B in the brain of Alzheimer patients, demonstrated by [^{11}C]-l-deprenyl using whole hemisphere autoradiography. *Neurochem Int* **58**, 60-68.
- [30] Carter SF, Chiotis K, Nordberg A, Rodriguez-Vieitez E (2019) Longitudinal association between astrocyte function and glucose metabolism in autosomal dominant Alzheimer's disease. *Eur J Nucl Med Mol Imaging* **46**, 348-356.
- [31] Banati RB, Newcombe J, Gunn RN, Cagnin A, Turkheimer F, Heppner F, Price G, Wegner F, Giovannoni G, Miller DH, Perkin GD, Smith T, Hewson AK, Bydder G, Kreutzberg GW, Jones T, Cuzner ML, Myers R (2000) The peripheral benzodiazepine binding site in the brain in multiple sclerosis: Quantitative *in vivo* imaging of microglia as a measure of disease activity. *Brain* **123** (Pt 11), 2321-2337.
- [32] Papadopoulos V, Baraldi M, Guilarte TR, Knudsen TB, Lacapere JJ, Lindemann P, Norenberg MD, Nutt D, Weizman A, Zhang MR, Gavish M (2006) Translocator protein (18kDa): New nomenclature for the peripheral-type benzodiazepine receptor based on its structure and molecular function. *Trends Pharmacol Sci* **27**, 402-409.
- [33] Cagnin A, Brooks D, Kennedy A, Gunn R, Myers R, Turkheimer F, Jones T, Banati R (2001) *In-vivo* measurement of activated microglia in dementia. *Lancet* **358**, 461-467.
- [34] Yasuno F, Ota M, Kosaka J, Ito H, Higuchi M, Doronbekov TK, Nozaki S, Fujimura Y, Koeda M, Asada T, Sahara T (2008) Increased binding of peripheral benzodiazepine receptor in Alzheimer's disease measured by positron emission tomography with [^{11}C]DAA1106. *Biol Psychiatry* **64**, 835-841.
- [35] Kreisl WC, Lyoo CH, McGwier M, Snow J, Jenko KJ, Kimura N, Corona W, Morse CL, Zoghbi SS, Pike VW, McMahon FJ, Turner RS, Innis RB (2013) *In vivo* radioligand binding to translocator protein correlates with severity of Alzheimer's disease. *Brain* **136**, 2228-2238.
- [36] Varrone A, Oikonen V, Forsberg A, Joutsa J, Takano A, Solin O, Haaparanta-Solin M, Nag S, Nakao R, Al-Tawil N, Wells LA, Rabiner EA, Valencia R, Schultze-Mosgau M, Thiele A, Vollmer S, Dyrks T, Lehmann L, Heinrich T, Hoffmann A, Nordberg A, Halldin C, Rinne JO (2015) Positron emission tomography imaging of the 18-kDa translocator protein (TSPO) with [^{18}F]FEMPA in Alzheimer's disease patients and control subjects. *Eur J Nucl Med Mol Imaging* **42**, 438-446.
- [37] Fan Z, Calsolaro V, Atkinson RA, Femminella GD, Waldman A, Buckley C, Trigg W, Brooks DJ, Hinz R, Edison P (2016) Flutriciclamide (18F-GE180) PET: First-in-human PET study of novel third-generation *in vivo* marker of human translocator protein. *J Nucl Med* **57**, 1753-1759.
- [38] Hamelin L, Lagarde J, Dorothee G, Leroy C, Labit M, Comley RA, de Souza LC, Corne H, Dauphinet L, Bertoux M, Dubois B, Gervais P, Colliot O, Potier MC, Bottlaender M, Sarazin M, Clinical IMABio3 team (2016) Early and protective microglial activation in Alzheimer's disease: A prospective study using 18F-DPA-714 PET imaging. *Brain* **139**, 1252-1264.
- [39] Wiley CA, Lopresti BJ, Venneti S, Price J, Klunk WE, DeKosky ST, Mathis CA (2009) Carbon 11-labeled Pittsburgh Compound B and carbon 11-labeled (R)-PK11195 positron emission tomographic imaging in Alzheimer disease. *Arch Neurol* **66**, 60-67.
- [40] Okello A, Edison P, Archer HA, Turkheimer FE, Kennedy J, Bullock R, Walker Z, Kennedy A, Fox N, Rossor M, Brooks DJ (2009) Microglial activation and amyloid deposition in mild cognitive impairment: A PET study. *Neurology* **72**, 56-62.
- [41] Schuitmaker A, Kropholler MA, Boellaard R, van der Flier WM, Kloet RW, van der Doef TF, Knol DL, Windhorst AD, Luurtsema G, Barkhof F, Jonker C, Lammertsma AA, Scheltens P, van Berckel BN (2013) Microglial activation in Alzheimer's disease: An (R)-[(^{11}C)]PK11195 positron emission tomography study. *Neurobiol Aging* **34**, 128-136.
- [42] Venneti S, Lopresti BJ, Wang G, Hamilton RL, Mathis CA, Klunk WE, Apte UM, Wiley CA (2009) PK11195 labels activated microglia in Alzheimer's disease and *in vivo* in a mouse model using PET. *Neurobiol Aging* **30**, 1217-1226.
- [43] Owen DR, Yeo AJ, Gunn RN, Song K, Wadsworth G, Lewis A, Rhodes C, Pulford DJ, Bennacef I, Parker CA, StJean PL, Cardon LR, Mooser VE, Matthews PM, Rabiner EA, Rubio JP (2012) An 18-kDa translocator protein (TSPO) polymorphism explains differences in binding affinity of the PET radioligand PBR28. *J Cereb Blood Flow Metab* **32**, 1-5.
- [44] Fan Z, Okello AA, Brooks DJ, Edison P (2015) Longitudinal influence of microglial activation and amyloid on neuronal function in Alzheimer's disease. *Brain* **138**, 3685-3698.

- [45] Ni R, Marutle A, Nordberg A (2013) Modulation of $\alpha 7$ nicotinic acetylcholine receptor and fibrillar amyloid- β interactions in Alzheimer's disease brain. *J Alzheimers Dis* **33**, 841-851.
- [46] O'Callaghan JP (2002) Measurement of glial fibrillary acidic protein. *Curr Protoc Toxicol* **Chapter 12**, Unit 12.8.
- [47] Whitwell JL, Dickson DW, Murray ME, Weigand SD, Tosakulwong N, Senjem ML, Knopman DS, Boeve BF, Parisi JE, Petersen RC, Jack CR, Jr., Josephs KA (2012) Neuroimaging correlates of pathologically defined subtypes of Alzheimer's disease: A case-control study. *Lancet Neurol* **11**, 868-877.
- [48] Perez-Nievas BG, Stein TD, Tai HC, Dols-Icardo O, Scotton TC, Barroeta-Espar I, Fernandez-Carballo L, de Munain EL, Perez J, Marquie M, Serrano-Pozo A, Froesch MP, Lowe V, Parisi JE, Petersen RC, Ikonovic MD, Lopez OL, Klunk W, Hyman BT, Gomez-Isla T (2013) Dissecting phenotypic traits linked to human resilience to Alzheimer's pathology. *Brain* **136**, 2510-2526.
- [49] Shinohara M, Fujitoka S, Murray ME, Wojtas A, Baker M, Rovelet-Lecrux A, Rademakers R, Das P, Parisi JE, Graff-Radford NR, Petersen RC, Dickson DW, Bu G (2014) Regional distribution of synaptic markers and APP correlate with distinct clinicopathological features in sporadic and familial Alzheimer's disease. *Brain* **137**, 1533-1549.
- [50] Marutle A, Gillberg PG, Bergfors A, Yu W, Ni R, Nennesmo I, Voytenko L, Nordberg A (2013) (3)H-deprenyl and (3)H-PIB autoradiography show different laminar distributions of astroglia and fibrillar beta-amyloid in Alzheimer brain. *J Neuroinflammation* **10**, 90.
- [51] Sabbagh MN, Schauble B, Anand K, Richards D, Murayama S, Akatsu H, Takao M, Rowe CC, Masters CL, Barthel H, Gertz HJ, Peters O, Rasgon N, Jovalekic A, Sabri O, Schulz-Schaeffer WJ, Seibyl J (2016) Histopathology and florbetaben PET in patients incorrectly diagnosed with Alzheimer's disease. *J Alzheimers Dis* **56**, 441-446.
- [52] Catafau AM, Bullich S, Seibyl JP, Barthel H, Ghetti B, Leverenz J, Ironside JW, Schulz-Schaeffer WJ, Hoffmann A, Sabri O (2016) Cerebellar amyloid-beta plaques: How frequent are they, and do they influence 18F-Florbetaben SUV ratios? *J Nucl Med* **57**, 1740-1745.
- [53] Doré V, Bullich S, Rowe CC, Bourgeat P, Konate S, Sabri O, Stephens AW, Barthel H, Fripp J, Masters CL, Dinkelsborg L, Salvado O, Villemagne VL, De Santi S (2019) Comparison of (18)F-florbetaben quantification results using the standard Centiloid, MR-based, and MR-less CapAIBL(®) approaches: Validation against histopathology. *Alzheimers Dement* **15**, 807-816.
- [54] Ni R, Gillberg PG, Bergfors A, Marutle A, Nordberg A (2013) Amyloid tracers detect multiple binding sites in Alzheimer's disease brain tissue. *Brain* **136**, 2217-2227.
- [55] Ni R, Gillberg PG, Bogdanovic N, Viitanen M, Myllykangas L, Nennesmo I, Langstrom B, Nordberg A (2017) Amyloid tracers binding sites in autosomal dominant and sporadic Alzheimer's disease. *Alzheimers Dement* **13**, 419-430.
- [56] Villemagne VL, Mulligan RS, Pejoska S, Ong K, Jones G, O'Keefe G, Chan JG, Young K, Tochon-Danguy H, Masters CL, Rowe CC (2012) Comparison of 11C-PiB and 18F-florbetaben for Abeta imaging in ageing and Alzheimer's disease. *Eur J Nucl Med Mol Imaging* **39**, 983-989.
- [57] Rowe CC, Doré V, Jones G, Baxendale D, Mulligan RS, Bullich S, Stephens AW, De Santi S, Masters CL, Dinkelsborg L, Villemagne VL (2017) (18)F-Florbetaben PET beta-amyloid binding expressed in Centiloids. *Eur J Nucl Med Mol Imaging* **44**, 2053-2059.
- [58] Ossenkoppele R, Jansen WJ, Rabinovici GD, Knol DL, van der Flier WM, van Berckel BN, Scheltens P, Visser PJ, Amyloid PET Study Group, Verfaillie SC, Zwan MD, Adriaanse SM, Lammertsma AA, Barkhof F, Jagust WJ, Miller BL, Rosen HJ, Landau SM, Villemagne VL, Rowe CC, Lee DY, Na DL, Seo SW, Sarazin M, Roe CM, Sabri O, Barthel H, Koglin N, Hodges J, Leyton CE, Vandenberghe R, van Laere K, Drzezga A, Forster S, Grimmer T, Sanchez-Juan P, Carril JM, Mok V, Camus V, Klunk WE, Cohen AD, Meyer PT, Hellwig S, Newberg A, Frederiksen KS, Fleisher AS, Mintun MA, Wolk DA, Nordberg A, Rinne JO, Chetelat G, Lleo A, Blesa R, Fortea J, Madsen K, Rodrigue KM, Brooks DJ (2015) Prevalence of amyloid PET positivity in dementia syndromes: A meta-analysis. *JAMA* **313**, 1939-1949.
- [59] Kol A, Adamsky A, Groysman M, Kreisel T, London M, Goshen I (2020) Astrocytes contribute to remote memory formation by modulating hippocampal-cortical communication during learning. *Nat Neurosci* **23**, 1229-1239.
- [60] Verkhatsky A, Marutle A, Rodriguez-Arellano JJ, Nordberg A (2014) Gliial asthenia and functional paralysis: A new perspective on neurodegeneration and Alzheimer's disease. *Neuroscientist* **21**, 552-568.
- [61] Srinivasan K, Friedman BA, Larson JL, Lauffer BE, Goldstein LD, Appling LL, Borneo J, Poon C, Ho T, Cai F, Steiner P, van der Brug MP, Modrusan Z, Kaminker JS, Hansen DV (2016) Untangling the brain's neuroinflammatory and neurodegenerative transcriptional responses. *Nat Commun* **7**, 11295.
- [62] Habib N, McCabe C, Medina S, Varshavsky M, Kitsberg D, Dvir-Szternfeld R, Green G, Dionne D, Nguyen L, Marshall JL, Chen F, Zhang F, Kaplan T, Regev A, Schwartz M (2020) Disease-associated astrocytes in Alzheimer's disease and aging. *Nat Neurosci* **23**, 701-706.
- [63] Chun H, Im H, Kang YJ, Kim Y, Shin JH, Won W, Lim J, Ju Y, Park YM, Kim S, Lee SE, Lee J, Woo J, Hwang Y, Cho H, Jo S, Park J-H, Kim D, Kim DY, Seo J-S, Gwag BJ, Kim YS, Park KD, Kaang B-K, Cho H, Ryu H, Lee CJ (2020) Severe reactive astrocytes precipitate pathological hallmarks of Alzheimer's disease via H2O2- production. *Nat Neurosci* **23**, 1555-1566.
- [64] Jossan SS, Gillberg PG, d'Argy R, Aquilonius SM, Langstrom B, Halldin C, Oreland L (1991) Quantitative localization of human brain monoamine oxidase B by large section autoradiography using L-[3H]deprenyl. *Brain Res* **547**, 69-76.
- [65] Tong J, Meyer JH, Furukawa Y, Boileau I, Chang LJ, Wilson AA, Houle S, Kish SJ (2013) Distribution of monoamine oxidase proteins in human brain: Implications for brain imaging studies. *J Cereb Blood Flow Metab* **33**, 863-871.
- [66] Rodriguez-Vieitez E, Ni R, Gulyas B, Toth M, Haggkvist J, Halldin C, Voytenko L, Marutle A, Nordberg A (2015) Astrocytosis precedes amyloid plaque deposition in Alzheimer APPsw transgenic mouse brain: A correlative positron emission tomography and *in vitro* imaging study. *Eur J Nucl Med Mol Imaging* **42**, 1119-1132.
- [67] Kamphuis W, Middeldorp J, Kooijman L, Sluijs JA, Kooij EJ, Moeton M, Fieriks M, Mizee MR, Hol EM (2014) Glial fibrillary acidic protein isoform expression in plaque related astrogliosis in Alzheimer's disease. *Neurobiol Aging* **35**, 492-510.

- [68] Braak H, Braak E (1991) Neuropathological staging of Alzheimer-related changes. *Acta Neuropathol* **82**, 239-259.
- [69] Lemoine L, Saint-Aubert L, Nennesmo I, Gillberg PG, Nordberg A (2017) Cortical laminar tau deposits and activated astrocytes in Alzheimer's disease visualised by (3)H-THK5117 and (3)H-deprenyl autoradiography. *Sci Rep* **7**, 45496.
- [70] Villemagne VL, Fodero-Tavoletti MT, Masters CL, Rowe CC (2015) Tau imaging: Early progress and future directions. *Lancet Neurol* **14**, 114-124.
- [71] Parbo P, Ismail R, Hansen KV, Amidi A, Mårup FH, Gottrup H, Brændgaard H, Eriksson BO, Eskildsen SF, Lund TE, Tietze A, Edison P, Pavese N, Stokholm MG, Borghammer P, Hinz R, Aanerud J, Brooks DJ (2017) Brain inflammation accompanies amyloid in the majority of mild cognitive impairment cases due to Alzheimer's disease. *Brain* **140**, 2002-2011.
- [72] Fan Z, Aman Y, Ahmed I, Chetelat G, Landeau B, Ray Chaudhuri K, Brooks DJ, Edison P (2015) Influence of microglial activation on neuronal function in Alzheimer's and Parkinson's disease dementia. *Alzheimers Dement* **11**, 608-621.e607.
- [73] James ML, Belichenko NP, Shuhendler AJ, Hoehne A, Andrews LE, Condon C, Nguyen TV, Reiser V, Jones P, Trigg W, Rao J, Gambhir SS, Longo FM (2017) [(18)F]GE-180 PET detects reduced microglia activation after LM11A-31 therapy in a mouse model of Alzheimer's disease. *Theranostics* **7**, 1422-1436.
- [74] Kreisl WC, Lyoo CH, Liow JS, Wei M, Snow J, Page E, Jenko KJ, Morse CL, Zoghbi SS, Pike VW, Turner RS, Innis RB (2016) (11)C-PBR28 binding to translocator protein increases with progression of Alzheimer's disease. *Neurobiol Aging* **44**, 53-61.
- [75] Gulyás B, Vas A, Tóth M, Takano A, Varrone A, Cselényi Z, Schain M, Mattsson P, Halldin C (2011) Age and disease related changes in the translocator protein (TSPO) system in the human brain: Positron emission tomography measurements with [(11)C]vinpocetine. *Neuroimage* **56**, 1111-1121.
- [76] Hamelin L, Lagarde J, Dorothée G, Potier MC, Corlier F, Kuhnast B, Caillé F, Dubois B, Fillon L, Chupin M, Botlaender M, Sarazin M (2018) Distinct dynamic profiles of microglial activation are associated with progression of Alzheimer's disease. *Brain* **141**, 1855-1870.
- [77] Ghadery C, Koshimori Y, Coakeley S, Harris M, Rusjan P, Kim J, Houle S, Strafella AP (2017) Microglial activation in Parkinson's disease using [(18)F]-FEPPA. *J Neuroinflammation* **14**, 8.
- [78] Zhang MR, Kumata K, Maeda J, Yanamoto K, Hatori A, Okada M, Higuchi M, Obayashi S, Suhara T, Suzuki K (2007) 11C-AC-5216: A novel PET ligand for peripheral benzodiazepine receptors in the primate brain. *J Nucl Med* **48**, 1853-1861.
- [79] Boche D, Gerhard A, Rodriguez-Vieitez E (2019) Prospects and challenges of imaging neuroinflammation beyond TSPO in Alzheimer's disease. *Eur J Nucl Med Mol Imaging* **46**, 2831-2847.
- [80] Zanotti-Fregonara P, Pascual B, Veronese M, Yu M, Beers D, Appel SH, Masdeu JC (2019) Head-to-head comparison of (11)C-PBR28 and (11)C-ER176 for quantification of the translocator protein in the human brain. *Eur J Nucl Med Mol Imaging* **46**, 1822-1829.
- [81] Harada R, Hayakawa Y, Ezura M, Lerdsiriruk P, Du Y, Ishikawa Y, Iwata R, Shidahara M, Ishiki A, Kikuchi A, Arai H, Kudo Y, Yanai K, Furumoto S, Okamura N (2020) (18)F-SMBT-1: A selective and reversible positron-emission tomography tracer for monoamine oxidase-B imaging. *J Nucl Med* **62**, 253-258.
- [82] Pannell M, Economopoulos V, Wilson TC, Kersemans V, Isenegger PG, Larkin JR, Smart S, Gilchrist S, Gouverneur V, Sibson NR (2020) Imaging of translocator protein upregulation is selective for pro-inflammatory polarized astrocytes and microglia. *Glia* **68**, 280-297.
- [83] Tourmier BB, Tsartalis S, Ceyzériat K, Medina Z, Fraser BH, Grégoire MC, Kövari E, Millet P (2020) Fluorescence-activated cell sorting to reveal the cell origin of radioligand binding. *J Cereb Blood Flow Metab* **40**, 1242-1255.
- [84] Rabinovici GD, Furst AJ, Alkalay A, Racine CA, O'Neil JP, Janabi M, Baker SL, Agarwal N, Bonasera SJ, Mormino EC, Weiner MW, Gorno-Tempini ML, Rosen HJ, Miller BL, Jagust WJ (2010) Increased metabolic vulnerability in early-onset Alzheimer's disease is not related to amyloid burden. *Brain* **133**, 512-528.
- [85] Schöll M, Ossenkoppele R, Strandberg O, Palmqvist S, Jögi J, Ohlsson T, Smith R, Hansson O (2017) Distinct 18F-AV-1451 tau PET retention patterns in early- and late-onset Alzheimer's disease. *Brain* **140**, 2286-2294.
- [86] Ferreira D, Nordberg A, Westman E (2020) Biological subtypes of Alzheimer disease. A systematic review and meta-analysis. *Neurology* **94**, 436-448.
- [87] Fowler JS, Volkow ND, Wang GJ, Logan J, Pappas N, Shea C, MacGregor R (1997) Age-related increases in brain monoamine oxidase B in living healthy human subjects. *Neurobiol Aging* **18**, 431-435.
- [88] Fan Z, Brooks DJ, Okello A, Edison P (2017) An early and late peak in microglial activation in Alzheimer's disease trajectory. *Brain* **140**, 792-803.
- [89] Nagele RG, Wegiel J, Venkataraman V, Imaki H, Wang K-C, Wegiel J (2004) Contribution of glial cells to the development of amyloid plaques in Alzheimer's disease. *Neurobiol Aging* **25**, 663-674.
- [90] Palmqvist S, Schöll M, Strandberg O, Mattsson N, Stomrud E, Zetterberg H, Blennow K, Landau S, Jagust W, Hansson O (2017) Earliest accumulation of β -amyloid occurs within the default-mode network and concurrently affects brain connectivity. *Nat Commun* **8**, 1214.
- [91] Buckner RL, Sepulcre J, Talukdar T, Krienen FM, Liu H, Hedden T, Andrews-Hanna JR, Sperling RA, Johnson KA (2009) Cortical hubs revealed by intrinsic functional connectivity: Mapping, assessment of stability, and relation to Alzheimer's disease. *J Neurosci* **29**, 1860-1873.
- [92] Sepulcre J, Schultz AP, Sabuncu M, Gomez-Isla T, Chhatwal J, Becker A, Sperling R, Johnson KA (2016) *In vivo* tau, amyloid, and gray matter profiles in the aging brain. *J Neurosci* **36**, 7364-7374.
- [93] Petrella JR, Sheldon FC, Prince SE, Calhoun VD, Doraiswamy PM (2011) Default mode network connectivity in stable vs progressive mild cognitive impairment. *Neurology* **76**, 511-517.
- [94] Pereira JB, Ossenkoppele R, Palmqvist S, Strandberg TO, Smith R, Westman E, Hansson O (2019) Amyloid and tau accumulate across distinct spatial networks and are differentially associated with brain connectivity. *eLife* **8**, e50830.
- [95] Hoening MC, Bischof GN, Seemiller J, Hammes J, Kukulja J, Onur ÖA, Jessen F, Fliessbach K, Neumaier B, Fink GR, van Eimeren T, Drzezga A (2018) Networks of tau distribution in Alzheimer's disease. *Brain* **141**, 568-581.

- [96] Passamonti L, Tsvetanov KA, Jones PS, Bevan-Jones WR, Arnold R, Borchert RJ, Mak E, Su L, O'Brien JT, Rowe JB (2019) Neuroinflammation and functional connectivity in Alzheimer's disease: Interactive influences on cognitive performance. *J Neurosci* **39**, 7218-7226.
- [97] Leuzy A, Chiotis K, Lemoine L, Gillberg PG, Almkvist O, Rodriguez-Vieitez E, Nordberg A (2019) Tau PET imaging in neurodegenerative tauopathies-still a challenge. *Mol Psychiatry* **24**, 1112-1134.
- [98] Ono M, Sahara N, Kumata K, Ji B, Ni R, Koga S, Dickson DW, Trojanowski JQ, Lee VMY, Yoshida M, Hozumi I, Yoshiyama Y, van Swieten JC, Nordberg A, Suhara T, Zhang M-R, Higuchi M (2017) Distinct binding of PET ligands PBB3 and AV-1451 to tau fibril strains in neurodegenerative tauopathies. *Brain* **140**, 764-780.
- [99] Chen MK, Mecca AP, Naganawa M, Finnema SJ, Toyonaga T, Lin SF, Najafzadeh S, Ropchan J, Lu Y, McDonald JW, Michalak HR, Nabulsi NB, Arnsten AFT, Huang Y, Carson RE, van Dyck CH (2018) Assessing synaptic density in Alzheimer disease with synaptic vesicle glycoprotein 2A positron emission tomographic imaging. *JAMA Neurol* **75**, 1215-1224.
- [100] Wang Y, Wang Q, Haldar JP, Yeh FC, Xie M, Sun P, Tu TW, Trinkaus K, Klein RS, Cross AH, Song SK (2011) Quantification of increased cellularity during inflammatory demyelination. *Brain* **134**, 3590-3601.
- [101] Wang Q, Wang Y, Liu J, Sutphen CL, Cruchaga C, Blazey T, Gordon BA, Su Y, Chen C, Shimony JS, Ances BM, Cairns NJ, Fagan AM, Morris JC, Benzinger TLS (2019) Quantification of white matter cellularity and damage in preclinical and early symptomatic Alzheimer's disease. *Neuroimage Clin* **22**, 101767.
- [102] Ismail R, Parbo P, Madsen LS, Hansen AK, Hansen KV, Schaldemose JL, Kjeldsen PL, Stokholm MG, Gottrup H, Eskildsen SF, Brooks DJ (2020) The relationships between neuroinflammation, beta-amyloid and tau deposition in Alzheimer's disease: A longitudinal PET study. *J Neuroinflammation* **17**, 151-151.